HUNGARIAN UNIVERSITY OF AGRICULTURE AND LIFE SCIENCES

Diffusion bonding for fusion reactor conditions

DOI: 10.54598/001720

PhD thesis

Baross Tétény

Gödöllő

2021

Doctoral school

denomination: Mechanical Engineering PhD School

Science: Agricultural Engineering

Leader: Prof. Dr. Kalácska Gábor, DSc
Hungarian University of Agriculture and Life Sciences
Institute of Technology, MATE,
Szent István Campus Gödöllő
Department of Mechatronics

Supervisor: Prof. Dr. Jánosi László, CSc
Hungarian University of Agriculture and Life Sciences
Institute of Technology, MATE
Szent István Campus Gödöllő
Department of Mechatronics

Co-supervisor: Dr. Veres Gábor, DSc
Head of Department
Centre for Energy Research
Fusion Technology Department

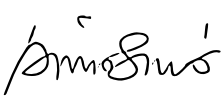

....

Affirmation of supervisor(s) Affirmation of head of school

CONTENTS

1. INTRODUCTION AND OBJECTIVES

In this chapter the significance and topics of my work are formulated.

1.1. Introduction

Nowadays, following the growing energy demand new, environmentally friendly power plants need to be developed. The ITER (International Thermonuclear Experimental Reactor) fusion reactor is aiming to demonstrate the scientific and technical feasibility of fusion as a new energy source.

The principle of the fusion process is that in the toroidal vacuum environment the charged particles (deuterium and tritium) are magnetically confined in a plasma state. After the collisions and fusion these particles will be transformed to helium and a will produce a high energy neutron. The released energy will be taken by the first wall elements, called Blanket Modules. Through the coolant water the transported heat will produce electricity in the power plants. Beyond the thermal load there is high-intensity neutron radiation that hits the wall elements, and this is much higher in order of magnitude compared to what we may find in a regular nuclear power plant. This radiation damages and degrades the materials and the diffusion bonding, which, due to heat conductance, would be essential in a vacuum environment.

One of the major components in the ITER vacuum vessel are the Blanket Modules. The Modules' cooling channels are manufactured by HIP (Hot Isostatic Pressure) diffusion bonding process, which is a "solid state welding" (Goods, Puskar, 2011). This process is used when large flat surfaces need to be bonded together. Furthermore, this process is used to bond the materials with different mechanical / thermodynamical properties where a proper heat conduction is required. These bonded seams will be crucial not only for ITER, but also for other tokamaks in the future.

For a good quality of the bonding, a thorough control is required during the manufacturing process. The proper welding parameters depend on the material properties, the surface preparation, and where the contaminations and oxides significantly influence the welding quality.

1.2. Objectives

The goal of my research was to investigate the diffusion bonding process of the structural materials developed for the ITER. Beyond the standard material investigations, I set alternative investigations as well. I also found it important to understand the theoretical calculations of diffusion bonding.

The diffusion bonding experiments were executed in the Gleeble laboratory at the University of Dunaújváros on a Gleeble 3800 Thermal-Mechanical

Physical Simulation System, which is suitable to investigate the bonding process in vacuum environment.

The diffusion bonding experiments were performed on specimens made from 316L as this material quality is the closest to the 316L(N)-IG developed for ITER.

Following the literature research, I did not find methods that were able to investigate the bonding process under the long diffusion process. The most important parameters of the diffusion bonding are the temperature, pressure, time and the surface roughness, where with the comparison of experiments and numerical simulations these parameters can be fine-tuned in the future. During the theoretical surface simulation of the diffusion bonding, it was visible that different mechanisms were dominant at different phases of the process. Therefore it may have a particular interest to investigate the bonding process in a direct way under the diffusion bonding.

To achieve this, I set the following objectives:

a) The physical simulation of diffusion bonding and monitoring the process on a thermo-mechanical physical simulator – Gleeble 3800. To carry out the diffusion bonding experiments made from two pieces, and the reference experiment from one specimen with the same parameters.

b) Preparation of a numerical modelling according to the Gleeble 3800 physical simulations in order to compare with the already measured results.

c) The comparison of the results between the theoretical modelling of the contact surface at the diffusion bonding and the physical experiments. This way to gain a better understanding of the theoretical model, and the investigation of the numerical modelling in correlation with the bonding parameters.

d) The research of the diffusion bonding under the experiments and with modelling instead of the stopped experiments at altering time intervals.

2. MATERIAL AND METHOD

In this chapter I present the experimental methods used to achieve my research goals and the thermal pre-calculations for the experiments, furthermore the calculation of the electrical resistance on the contact surface.

2.1. The diffusion bonding and the reference experiments

The diffusion bonding experiments were executed in the Gleeble laboratory at the University of Dunaújváros on the Gleeble 3800 Thermal-Mechanical Physical Simulation System. Comparing with other laboratory experiments in vacuum: the test specimens are not heated by heat radiation, but the current is lead through the specimens acting as a resistance heater. The experiment in the Gleeble cell can be seen on Fig. 1.

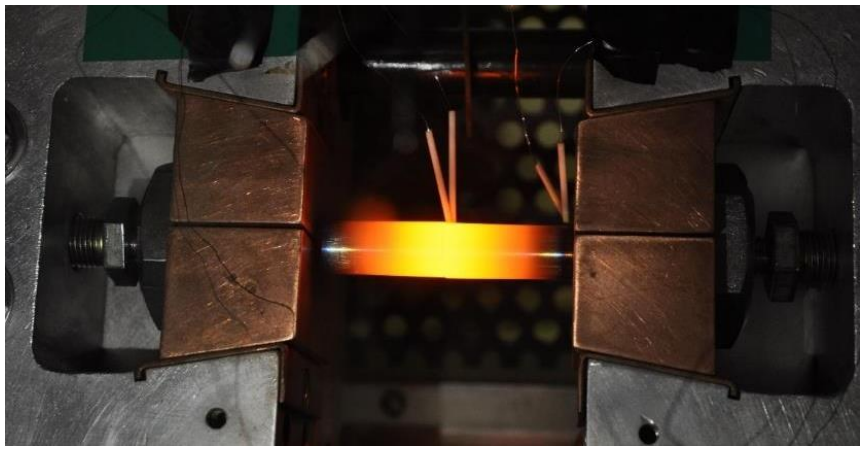

Figure 1. Diffusion bonding in the University of Dunaújváros Gleeble laboratory

Since the heat distribution has a reverse parabola characteristic the maximum temperature was measured in the middle (close to the bonded surfaces) and the minimum temperature close to the copper jaws. They were measured with two R-type thermocouples and the Gleeble system controlled the temperature according to the thermocouple close to the bonded surface. The axial load was set by the Quicksim software (with 10 Hz) to a pre-defined pressure and cross-section, ensuring the constant pressure on the bonded surface. Measured by a load cell the axial force was recorded, and similarly the Power Angle was recorded, which is used by the Gleeble control system. The pressure values in the vacuum chamber were recorded manually.

Diffusion bonding and reference experiments were executed with same parameters for comparison. The same circumstances were intended to ensure that the diffusion bonding gives the only difference between the two tests. The

316L specimens were manufactured from steel rods with 12,5 in diameter and 30 + 30 mm useful lengths. From the diffusion bonded and reference tests two pairs (four experiments) were selected for detailed investigation. These tests are summarized in Table 1.

Table 1. Physical simulations of diffusion bonding and reference specimens

Naming / Time on air	Diffusion bonding parameters			Left side	Right side	Original length	Length after tests
	T_{max} [°C]	P, MPa	t, min	Rz, µm	Rz, µm	mm	mm
DG3, 150 min	1000	30	60	0,58 / 0,93	0,6 / 0,59	30,07 + 30,02	58,48
RG3	1000	30	60			60,05	56,9
DG7, 120 min	1055	30	40	0,75 / 0,80	0,92 / 0,67	30,01 + 30,04	56,34
RG7, NA	1055	30	40			60,04	55,47

After the grinding of the surfaces as a preparation for bonding, the surface roughness was set in the range of $R_z = 0.5$ to 1 µm. After cleaning the Cr oxide was removed by CITRANOX ® acid solution. After a repeated surface cleaning the specimens were put and shipped in a vacuum chamber under Ar gas, preventing them from re-oxidation. However, due to the taking out and fixing them into the vacuum cell (lasted more than 60 mins), the oxidation could not be fully avoided, but presumably the oxide layer was much thinner compared to what the original surface had.

2.2. The thermal characteristics of the Gleeble experiments

I approximated the heat distribution of the specimens with 1D calculations, where the radial heat distribution caused by the heat radiation was checked by calculations as well. I found that despite of the significant heat radiation on a cylindrical specimen the 1D heat distribution gave a proper approximation, but the heat loss, due to the radiation, needs to be taken into account. The calculations showed that following the large heat difference the temperature dependent material properties need to be used for a precise numerical modelling. For the Gleeble experiments I prepared a 1D numerical model.

For the initially growing contact surface of the diffusion bonding, I have used the model developed by Hill and Wallach, and their so called 0. mechanism. According to the results the 30 MPa axial load gave about a 15 % contact surface at 1000 °C / 1050 °C. During the physical experiments in the heating up period we have applied 50 MPa axial pressure for a proper initial contact area before nominal axial pressure was used. This way the contact surface

melting could be avoided at the beginning of the physical experiments, and at the same time the lower axial pressure between 800°C and 1000°C used during the experiments ensured a lower deformation.

2.3. Calculation of the contact electrical resistance in function of contact area

In reality due to the surface contaminations and oxide layers the arising mechanical contact is not identical with the electrical contact surfaces. Because of this the 0. mechanism – with the plastic deformation of the surface asperities – does not substitute the slow mechanism where the different diffusion processes are dominant between the grains. This way it is expected that the oxides will disappear slowly. Since the conducting contact area means a proper mechanical contact too, the electrical resistance can be a good indicator.

I have determined the theoretical calculations of the contact electrical resistance on the bonded surface based on the Zhang (2012) models. Half of the symmetric contact model used can be seen on Fig. 2. In the cylindrical coordinate system, the "h" means the bridge length, that is based on the surface roughness height, which resistance is specified as the electrical resistivity (ρ_1) enlarged by the oxide layer and the contaminations.

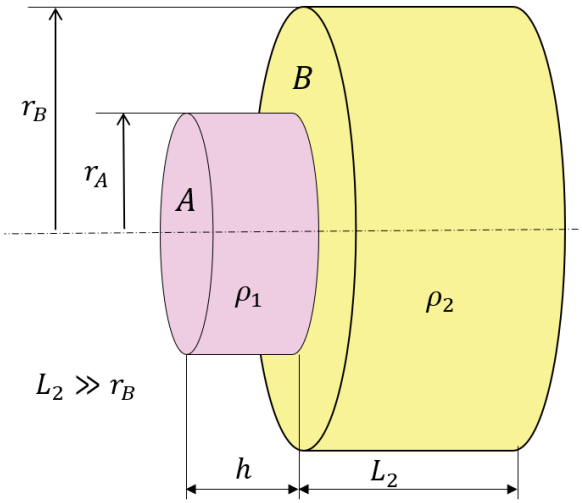

Figure 2. The current channel geometry for contact resistance by Zhang (2010)

The total resistance is the sum of the constriction resistance $R_{c\,A/B}$ and the bulk resistance arisen on the bridge R_h. Since I modelled a half specimen in heat distribution, the half of the contact resistance was determined.

$$R_{half\ contact} = R_h + R_{c\ A/B} = \frac{\rho_1 \cdot h}{\pi \cdot {r_A}^2} + \frac{\rho_2}{4 \cdot r_A} \cdot \bar{R}_{c\ A/B}\left(\frac{r_B}{r_A}, \frac{\rho_1}{\rho_2}\right), \quad (1)$$

where ρ_1 and ρ_2 are the specific electrical resistance (resistivity) of the bridge and base material. I have determined the constriction resistance based on the analytical equations by Zhang (2010, 2012). The calculations showed that the constriction resistance around the conducting areas may give much larger electrical resistance to the sum of the total as the resistance due to the oxide layers and contaminations, even if $\rho_1 = 100 * \rho_2$.

3. RESULTS

In this chapter, I present the results of my research, which helped me to determine the ratio of the contact area under the bonding process. I present the results of the theoretical model for contact surface growing modelled by Hill and Wallach (1989), and the contact surface was determined by the Zhang (2012) calculations based on the introduced contact resistance through the own modelling of the Gleeble experiments.

3.1. The evaluation of the diffusion bonding and the reference experiments

The parameters of the two chosen pairs of the experiments are detailed in Table 1. as DG7 / RG7 on 1055 °C / 30 MPa / 40 min and DG3 / RG3 on 1000 °C / 30 MPa / 60 min. All experiments had a heating up period with 540 s, a 2400 / 3600 s nominal bonding period and a controlled cooling period. The image of the DG3 / RG3 specimens after the experiments can be seen on Fig. 3.

Figure 3. The Gleeble specimens RG3 (reference experiment), DG3 (diffusion bonding specimen) with the same heat and axial load, below the initial pieces

The measured stroke functions of the four experiments are visible on Fig. 4., where for the comparison the beginnings of the diffusion procedures are shifted to one point. The measurements show smaller strokes on the diffusion bonded specimens compared to the reference tests without bonding surfaces using the same parameters. The measured stroke here means the axial deformation of a specimen. The measured temperatures are visible on Fig. 5.

We can assume that between the two specimens the only difference is the contact electrical resistance at the bonded contact surface. This significantly modifies the heat distribution, which impacted on the creep properties.

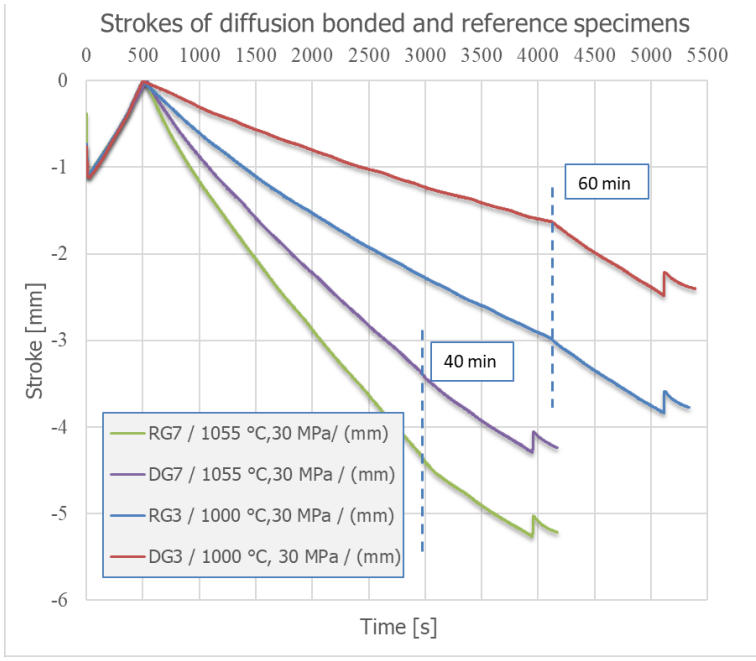

Figure 4. The strokes, axial deformations of the specimens during the diffusion bonding and the reference measurements

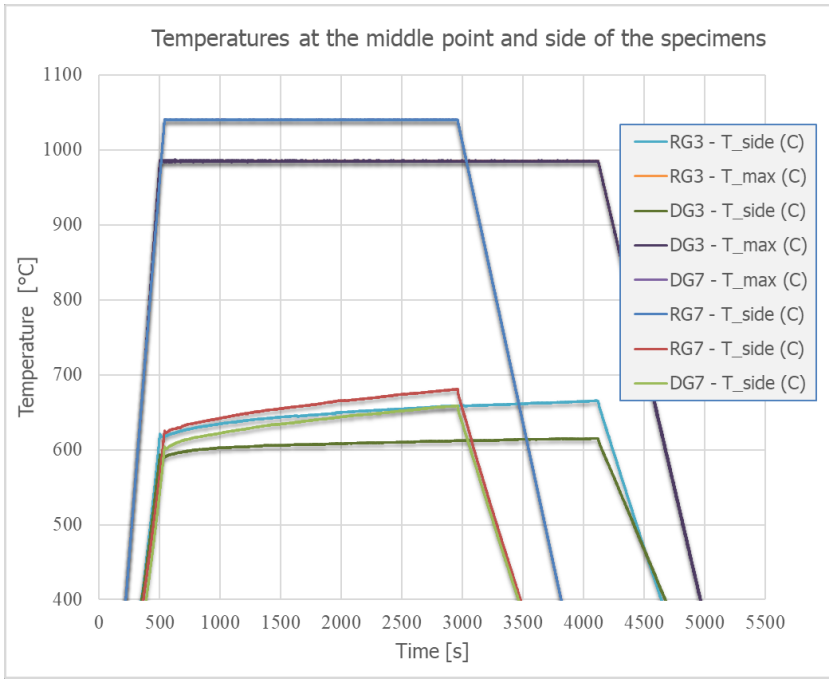

Figure 5. The measured temperature of the DG7 / RG7 and DG3 / RG3 experiments, heat up, diffusion bonding, controlled cooling

3.2. Numerical modelling of the Gleeble experiments

For the study I prepared a 1D heat distribution model for the experiments, which could calculate the heat distribution on the deformed specimens, and according to the axial compression, it modelled the axial deformation. During the long process the model was able to follow the heat generation and heat distribution according to the altering geometry. The numerical model controlled the DC current to set the constant temperature close to the bonded surfaces, and it controlled the axial load to ensure the constant surface pressure on the surfaces. In the model I approximated the axial deformation with a temperature dependent creep function. Fig. 6. shows the schematic view of the heat generation and the heat transport.

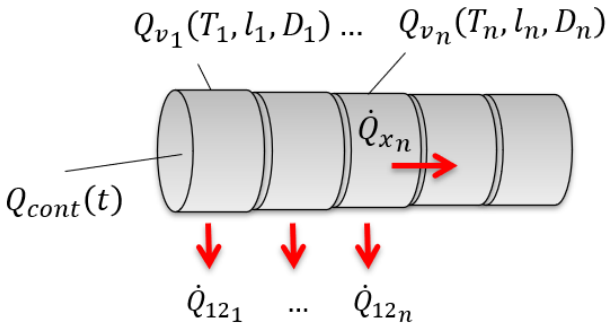

Figure 6. Heat generation and heat transport in a half specimen with contact

In a half specimen through the nth element from left the heat transport will be equal with the sum of the *1…nth* element heat generation reduced by the loss of the heat radiation: $\sum_1^n \dot{Q}_{x_n}$. This heat generation will be equal in steady state with the heat transport through one element. Assuming that the deformation is much slower than the heat transport, in the *kth* time step it can be written:

$$\sum_0^n \dot{Q}_{x_{n,k}} = \lambda(T_{n+1,k}) \cdot \frac{A_{n,k}}{l_{n,k}} (T_{n-1,k} - T_{n,k}), \qquad (2)$$

where $\lambda(T_n)$ is the thermal conductance of the *nth* element.

Close to the side of the specimen at the fixing, the measured temperature helped to define the heat transfer coefficient value between the specimen and the cooling water. The heat transfer through the jaws at $n = N$ will be the following:

$$\sum_{0}^{n=N} \dot{Q}_{x_{N,k}} = \alpha_{jaws} \cdot A_{N,k}\left(T_{N,k} - T_{cooling\ water}\right), \tag{3}$$

where $\alpha_{jaw} = 2000 - 4200$ W/(m^{2}K). After rearranging the equations, one gets the $T_{N,k}$, and $T_{n-1,k}$ values. The welding temperature is $T_{1,k}$.

Observed with naked eyes the revers parabolic heat distribution showed similarity during the experiments, but during the numerical modelling the difference is more observable. On Fig. 7. at 60 s and 2400 s for the DG3 / RG3, DG7 / RG7 experiments the heat distributions and the heat fluxes are visible, whereas through the bonding process the difference is reducing.

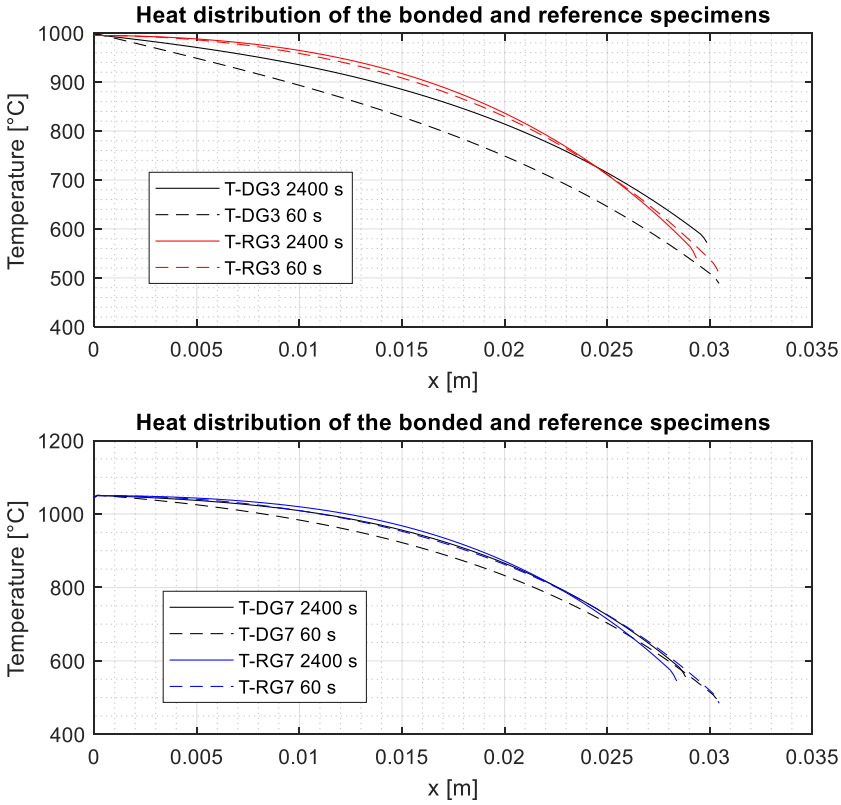

Figure 7. Heat distributions were calculated to the DG3 / RG3 DG6 / RG7 experiments in the numerical modelling at 60 s 2400 s (Baross et al, 2020)

The measured and modelled strokes are visible on Fig. 8. The increasing Power Angle and the controlled and modelled DC current are visible on Fig.

9. for DG7 / RG7 experiments. The block diagram of the numerical model can be seen on Fig. 10.

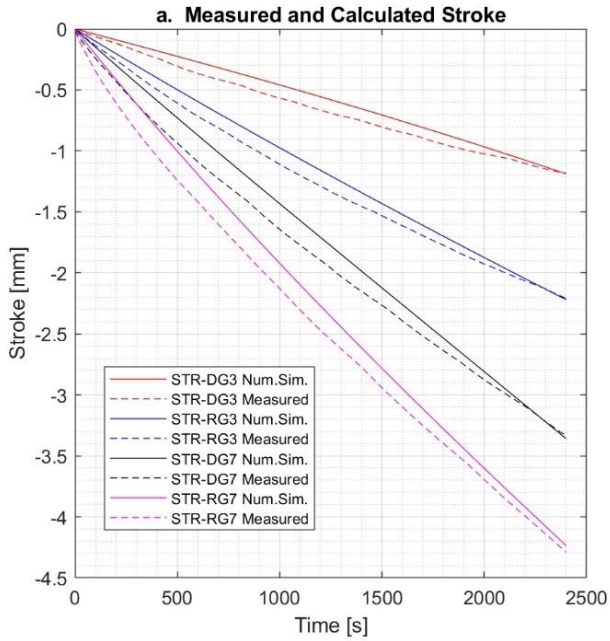

Figure 8. The measured and modelled stroke during the nominal period of the experiments for the four experiments (Baross et al, 2020)

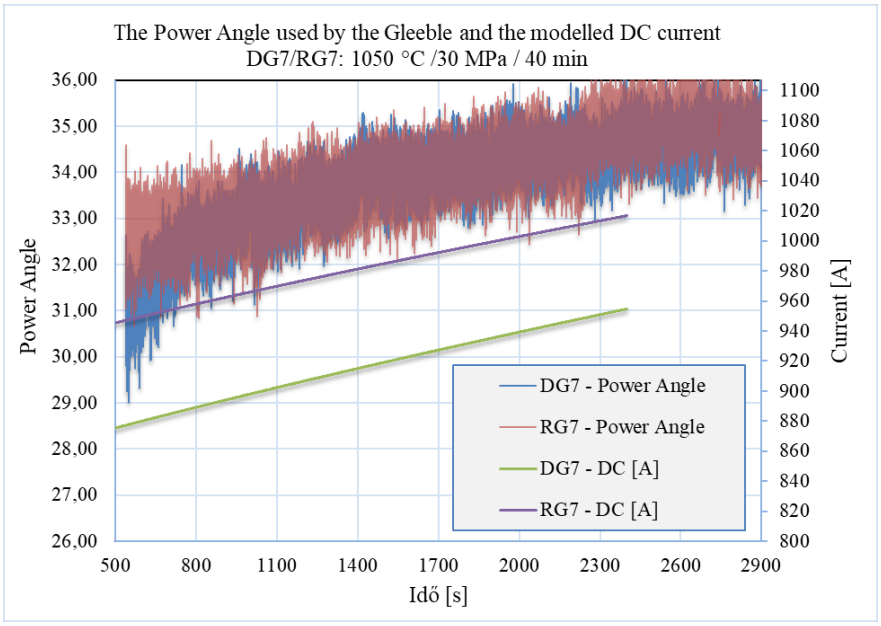

Figure 9. Increasing Power Angle and the modelled DC current of DG7 / RG7

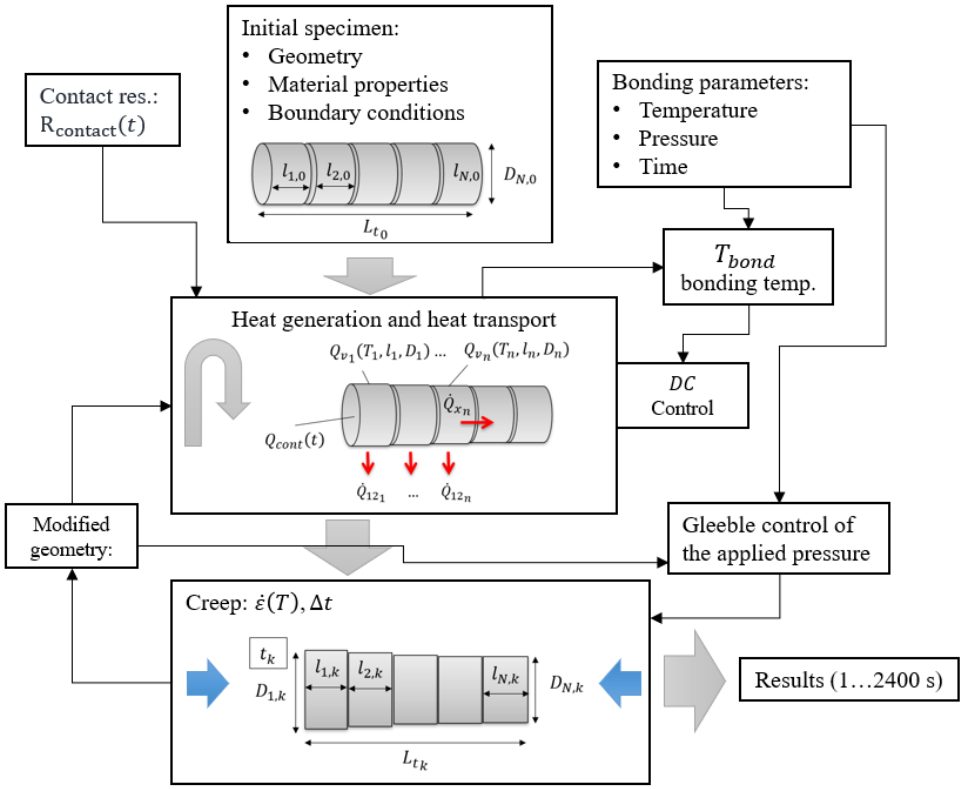

Figure 10. The block diagram of the numerical modelling

The cross-sections with discrete length were calculated with a constant volume, where based on the earlier studies (Hill, 1983, 1989, Rieth, 2004) the Arrhenius type creep equations were used on the dominantly high 950 °C – 1050 °C temperature regime. The exponent of the creep equation was adjusted to the reference experiments, and these creep functions were applied to the diffusion bonding experiments in the model as well. This way the only difference is the appeared contact electrical resistance could be investigated.

The increasing axial load on the axially shortened specimens showed less than 1% difference in the modelling and in the measurements, see Fig. 11.

In this way the numerical modelling was able to estimate the deformation of the specimens during the long experiments.

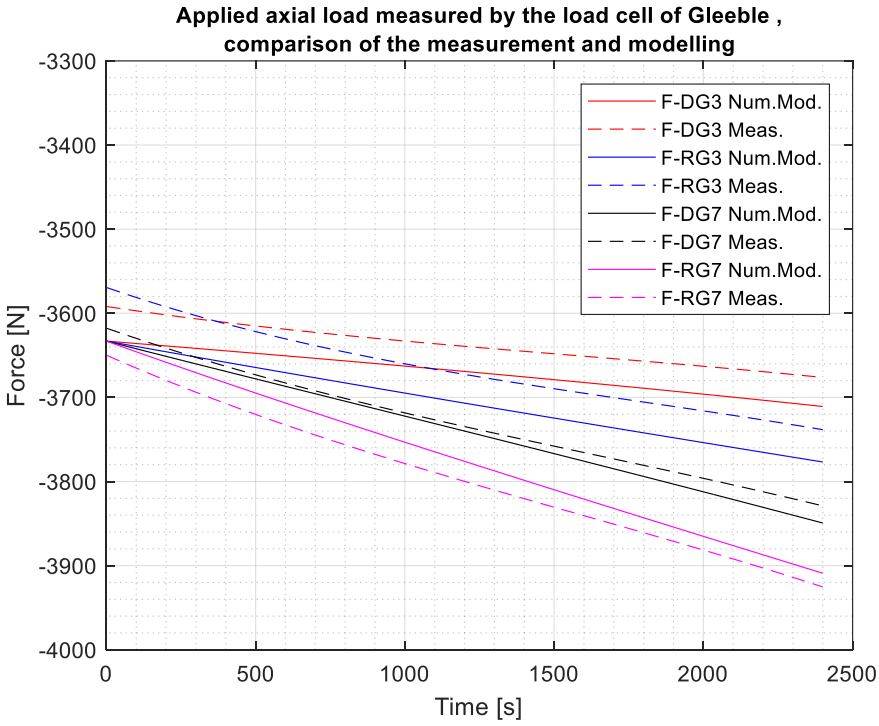

Figure 11. Comparison of the increasing axial load with num. modelling with the measured values

3.3. The contact electrical resistance

The increasing contact area during a diffusion bonding was approximated with a decreasing contact electrical resistance raised on the mating surfaces. The electrical resistance was added to the left side of the half specimen. Since this resistance could not be modelled as a function of a parameter, it is determined in time as a decreasing function. The exponential decreasing function was the following:

$$R_{contact} = k_1 \cdot e^{-k_2 \cdot t}, \tag{4}$$

where k_1 [Ω], k_2 [1/s] are the parameters of the function with which the characteristics of the stroke can be modified in the numerical modelling. The parameters were set to be equal to the measured stroke at the 40th minute.

The two functions of the contact electrical resistance derived for DG7 and DG3 are visible on the Fig. 12.

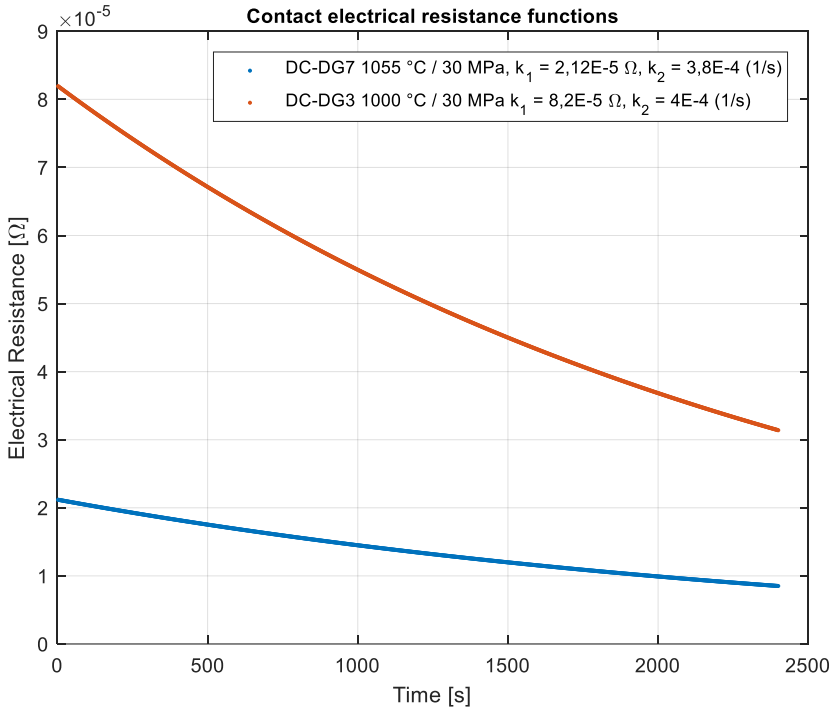

Figure 12. The functions (DG7, DG3) of the contact electrical resistance at the diffusion bonded derived by the numerical modelling

3.4. Determination of the contact surface area

I have determined the contact resistance function based on the Zhang (2012) equations in function of the A / B ratio (Fig. 2.). The electrical resistance function is visible on Fig. 13., where according to the eq. 1. its half value was determined.

The contact resistance decreases under 10^{-5} (Ohm) after reaching the 10% contact ratio. By this I showed that the contact electrical resistance (in time) determined from the Gleeble numerical modelling, and the contact resistance derived by the Zhang equations have the same order of magnitude and give comparable results. Hereby, through the contact electrical resistance function by the Gleeble experiments and modelling, and by the Zhang theoretical equations I determined the contact area in the function of time: $A/B(R_{contact}(t))$.

To define the A/B(t) I derived the $A/B(R_{contact})$ from the $R_{contact}(A/B)$. The function was approximated under the 10 x 10^{-5} order of magnitude with a polynomial for larger than 10% contact area. In reality, we can assume also larger than a 10% contact in the beginning of the bonding process as it was presented earlier. For DG3 and DG7 the ratio of the contact surface $A/B(R_{cont}(t))$ in time can be seen on Fig. 14.

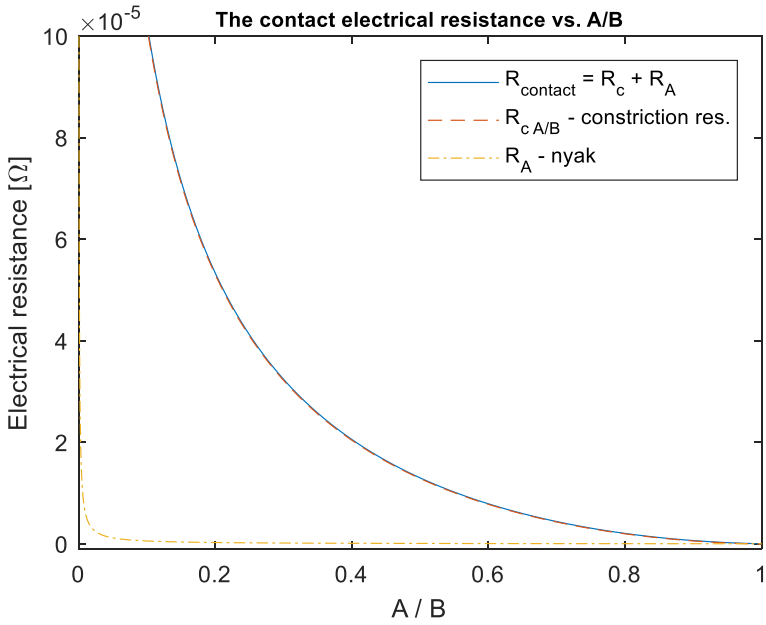

Figure 13. The contact electrical resistance in the function of A/B, surf. geometry: h = 0,12 μm; nominal radius of the contact: r_B = 6,25 mm; the contact area radius r_A = 0,05 ÷ 6,25 mm; ρ(1050 °C) = 1,256e-06 Ωm; $\rho_1/\rho_2 = 50$.

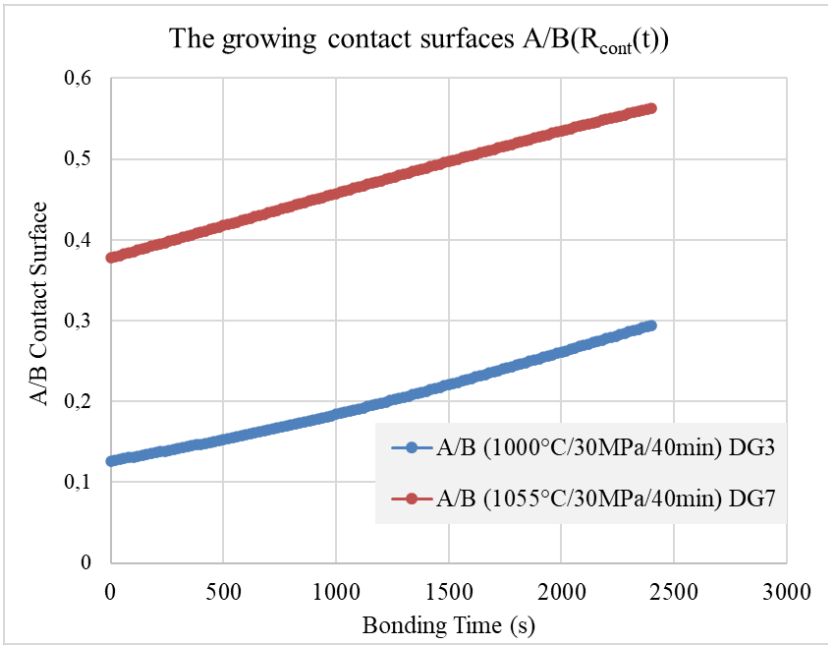

Figure 14. The growing ratio of contact surfaces A/B(R_{cont}(t)) for DG3 and DG7

3.5. The results of the Hill and Wallach diffusion model

I prepared the model based on the Hill and Wallach model. The model shows a significant contact grow at the beginning of the process, which is the result of the ideal characteristic of the different parallel mechanism. However, the experiences on tests in literature give a not satisfying mechanical contact, because of the oxidation and contamination on the surfaces. It is worth to note, if this could be reduced significantly the bonding quality would be much better. Since the pre-heating or baking of the surface could not be performed in the vacuum cell, we could expect some contamination and oxide layers on the surfaces.

Using the 316L material parameters in the Hill and Wallach model for the diffusion bonding we can get the model in function of the bonding parameters. The results of the plastic deformation according to the two experiments: DG3 / DG7 can be seen on the Fig. 16. (DG7) and Fig. 19. (DG3). The mechanisms and the sum of the ratio of the bonded area are visible on the Fig. 17. (DG7) and Fig. 19. (DG3). The quarter of the ellipse voids were calculated by the model during the two processes are visible on Fig. 18. (DG7) and on Fig. 21. (DG3).

At first step the Hill and Wallach model calculates the instantaneous plastic deformation (0. mechanism). With this we can estimate in the cell the contact area as a neck, which belongs to the yield stress at a certain temperature: a_{yield}, where the ellipse height will be the h_{yield}. The schematic view of the mechanism is visible on Fig. 15.

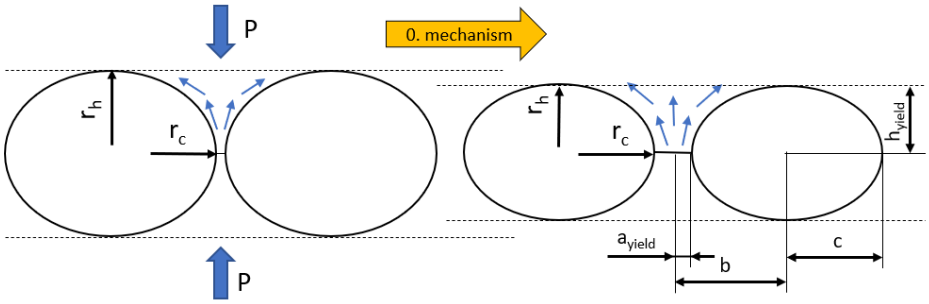

Figure 15. Material transport during the 0. mechanism, assuming an instantaneous plastic deformation

The Hill and Wallach model assumes symmetrical surface roughness profile, where the material transport remains in plane. The surface asperities replaced by ellipses, which joints perfectly symmetrical at their tips, “creating between them a series of infinitely long parallel cylinders of elliptical cross-section” (Hill and Wallach, 1989), where the surface has no waviness according to the theory. During plastic deformation the model do not assume work hardening. The 0. plastic mechanism is not time dependent. In the Table 2. showed

surface roughness parameters were derived from the measured roughness profiles of the actual specimens.

Table 2. Surface roughness parameters derived from the measured values

	Specimen Nr.		R_a (µm)	R_z (µm)	R_q (µm)	λ_a (µm)
DG7	Nr. 1.	1. meas.	0,06	0,75	0,08	23,24
		2. meas.	0,06	0,8	0,08	22,47
	Nr. 4.	1. meas.	0,09	0,92	0,13	28,42
		2. meas.	0,06	0,67	0,08	18,55
1055 °C /30 MPa / 40 min		Average	0,0675	0,785	0,0925	23,17
DG3	Nr. 8.	1. meas.	0,06	0,58	0,07	20,84
		2. meas.	0,06	0,93	0,08	20,46
	Nr. 11.	1. meas.	0,06	0,6	0,07	21,76
		2. meas.	0,06	0,59	0,07	22,13
1000 °C / 30 MPa / 40 min		Average	0,06	0,675	0,0725	21,30
Geometry ellipse input data		Grain size 20 µm			$h = 2\,R_q$	$2\,b = \lambda_a$

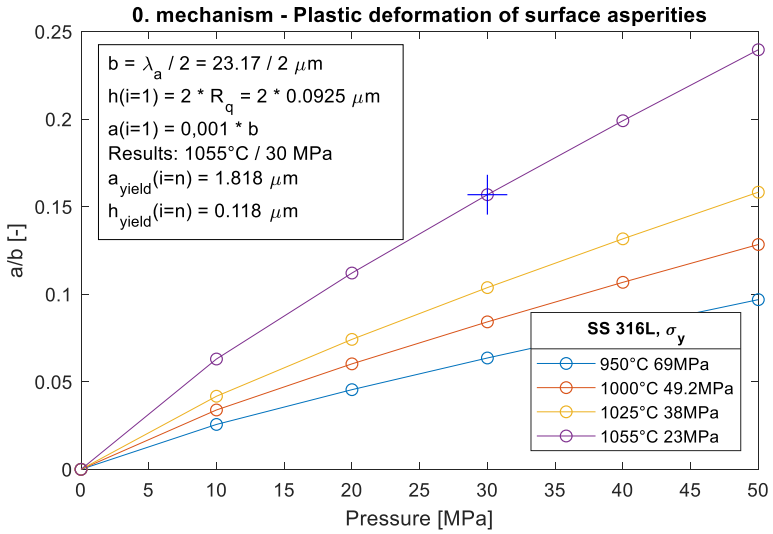

Figure 16. The DG7 (1055 °C / 30 MPa) results of the 0. mechanism instantaneous plastic deformation in function of different yield stresses and surface pressure, the h_{yield}, a_{yield} are used for the later 1-6 mechanisms

As the result of the plastic instantaneous deformation the Fig. 16. shows the ratio of the neck / unit cell: a/b. More results are show for comparison in the

range of 950 – 1055 °C. The cross marks the DG7 point, where I calculated 15% bonding ratio at 1055 °C. The h_{yield}, a_{yield} will be used for the later 1-6 mechanisms

After the initial mechanism the different parallel mechanisms, as diffusion, evaporation and condensation and the power-law creep mechanism will effectuate in the bonding with different rates. The results show that the surface diffusion mechanism will dominate on this temperature and pressure. The evaporation, diffusion between the grains, and the creep mechanism will contribute less. The main driving force to the surface mechanism is the elongated ellipse void shape, which tends to form a circle, which results an equilibrium state for the surface mechanisms. The quarter of the ellipse voids are visible on Fig. 18. (DG7) and Fig. 21. (DG3). The elongated voids form quickly to a circle during the initial part following the diffusional process, then the other mechanisms shall shrink the voids, which at the ends will disappear.

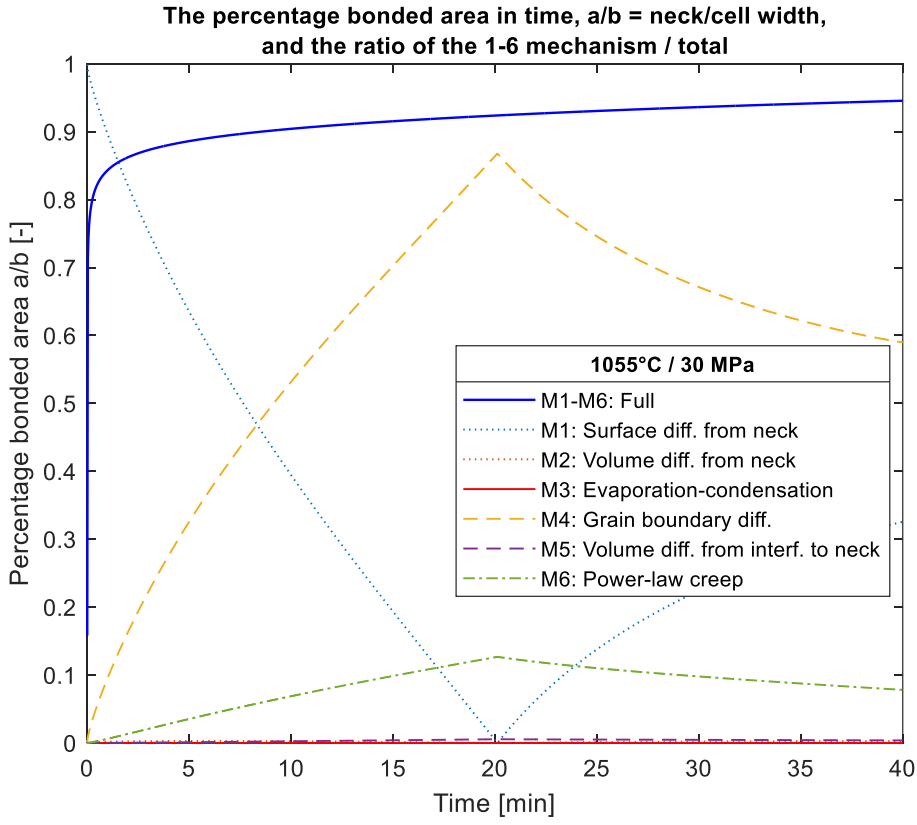

Figure 17. The DG7 (1055 °C / 30 MPa / 40 min) diffusion bonding main results of the 1-6 mechanism by the Hill and Wallach model, geometrical inputs: h_{yield} = 0,118 µm, a_{yield} = 1,818 µm, $2 \cdot b_0$ = 23.17 µm, grain size: 7 µm

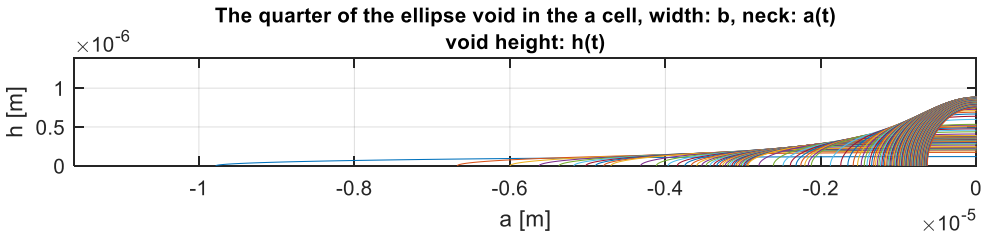

Figure 18. The void forming in the DG7 bonding model in a quarter cell, ellipse width: c(t), height: h(t), neck width: a(t)=b-c(t)

Fig. 19. shows the 0. mechanism of the DG3 similarly to DG7. The cross marks the DG3 diffusion bonding point result at 30 MPa, 1000 °C.

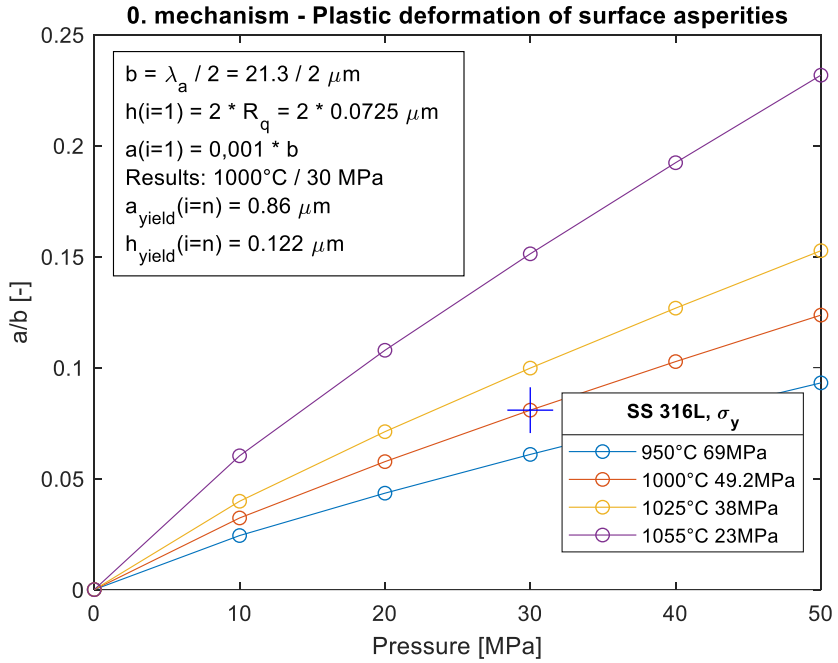

Figure 19. The DG3 (1000 °C / 30 MPa) results of the 0. mechanism instantaneous plastic deformation in function of different yield stresses and surface pressure, the h_{yield}, a_{yield} are used for the later 1-6 mechanisms

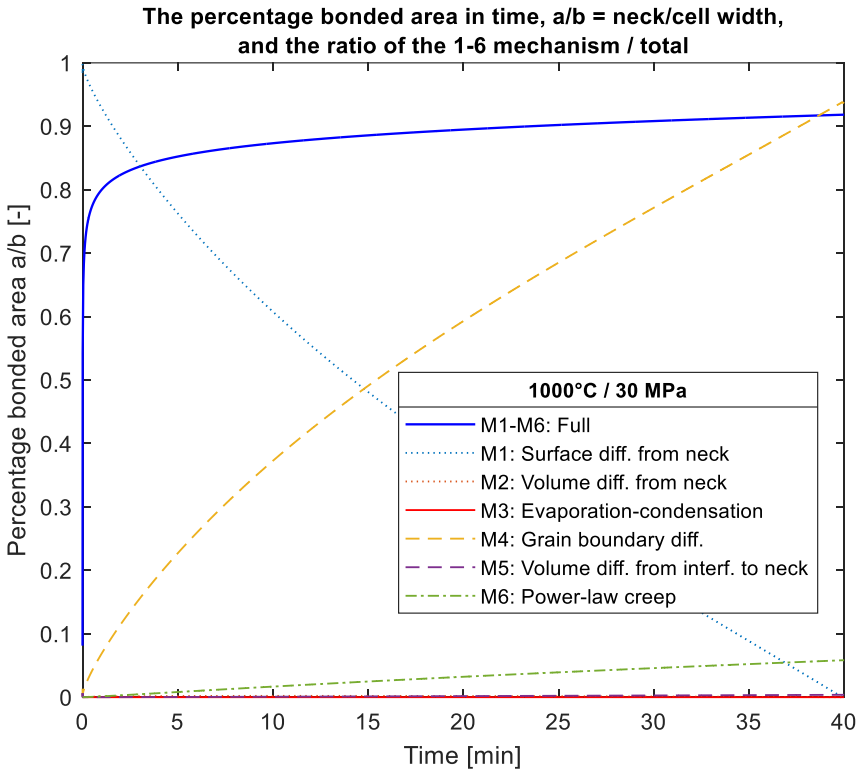

Figure 20. The DG3 (1000 °C / 30 MPa / 40 min) diffusion bonding main results of the 1-6 mechanism by the Hill and Wallach model, geometrical inputs: h_{yield} = 0,122 µm, a_{yield} = 0,86 µm, $2 \cdot b_0$ = 23.17 µm, grain size: 7 µm

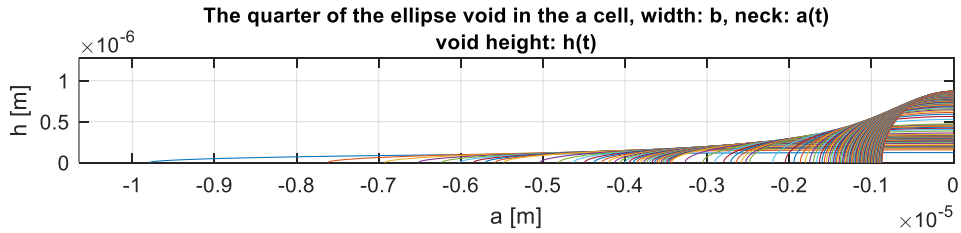

Figure 21. The void forming in the DG3 bonding model in a quarter cell, ellipse width: c(t), height: h(t), neck width: a(t)=b-c(t)

Summarizing the Hill and Wallach model, it shows a quick contact accordingly to the literature, assuming a clean surface, without any waviness. However, the “a” neck width grows quickly in both cases, but following the slower mechanisms at a lower temperature - in case of DG3 - the neck height “h” is decreasing slower compared to the diffusion bonding at DG7. In general, we can say that the elongated voids form quickly to a circle following

the initial mechanisms, then the 1-6 mechanisms shrink much slower the voids. According to the surface void modelling it is reasoned to keep the temperature at a high temperature (1050–1100 °C), as they can be found in the literature too, where to ensure the disappearing of the voids the process is held until 2 hours. However, the higher pressure may speed up the bonding process, but I did not intend to test it, because of the larger radial deformations of the specimens.

3.6. Comparing the bonded area of the theory and the numerical model

The theoretical diffusion bonded area (a/b) by the Hill and Wallach and the determined bonded ratio (A/B) from the measurements through the numerical modelling and with the Zhang equations are summarized in the Fig. 22.

The theoretical model and the experiments show higher bonded area at higher temperature in time, as it was expected. However, for an exact measurement we need to make fracture tests combined with microscope investigations.

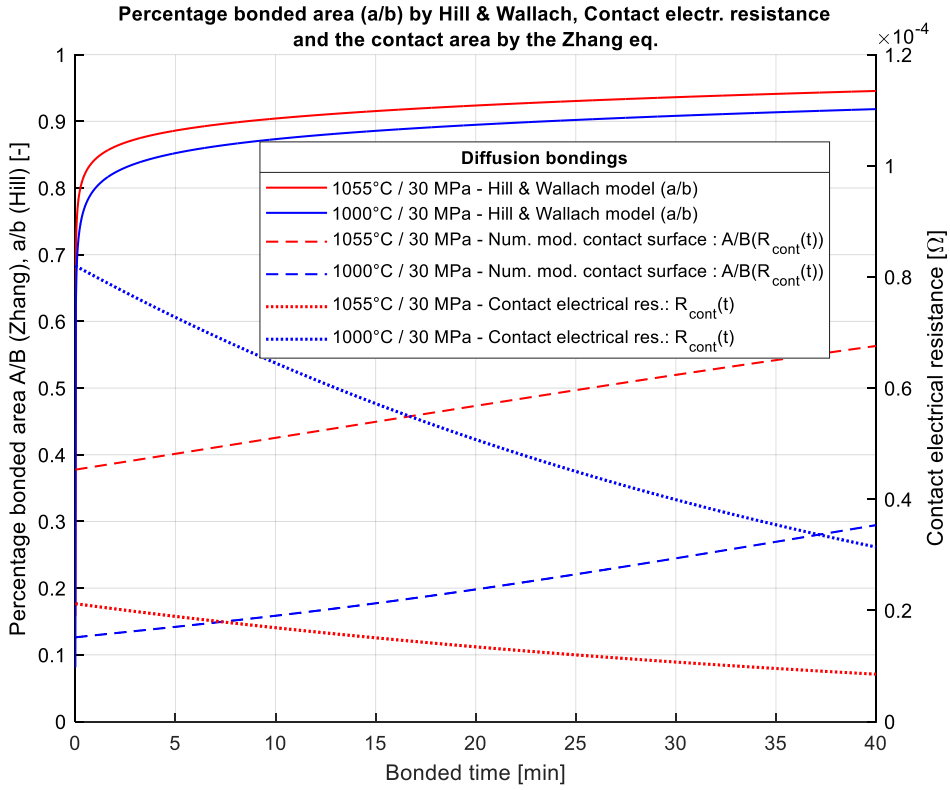

Figure 22. The diffusion bonded area (a/b) by the Hill and Wallach model comparing with the electr. resist. $R_{cont}(t)$ were derived by the numerical modelling, where the contact area derived by the Zhang eq.

The theoretical Hill and Wallach modelling of a/b and the measured and calculated A/B derived show significant difference, where the later give lower values. Taking into account the possible oxidation, contaminations I expected certainly lower results. Furthermore, according to the later corrected models for the Hill and Wallach model (1989) by Zhang, M. Q. Li (2015, 2018) and by Ruifang et al. (2012) gave for other alloys more realistic results. According to their results I think that in the future it shall be beneficial to investigate and apply the newer models for the 316L stainless steels too.

With these, I worked out a method through the measurements of the Gleeble to determine the bonded area during the diffusion bonding. I made comparable the bonded area between the theoretical Hill and Wallach model and the functions were determined by the developed numerical model and the Zhang equation.

4. NEW SCIENTIFIC RESULTS

The topic of my research was the diffusion bonding of 316L stainless steel specimens, that have grades very close to the structural materials used in present fusion reactors. I formulated my results in the following points.

1. *Investigation of the diffusion bonding process with a Gleeble physical simulator system*

I proved with experiments on 316L stainless steel specimens that the diffusion bonding experiments carried out by resistance heating together with the reference measurements are feasible to investigate the diffusion bonding process.

During the experiments I found a relationship between the dissimilar axial deformations of the bonded and reference specimens, and the diffusion bonding process on the mating surface.

The diffusion bonding and reference experiments were carried out with the same parameters at 1000 °C/ 30 MPa/ 60 min and 1055 °C/ 30 MPa/40 min.

I worked out a numerical model, which could model the heat distribution on the specimen and the axial and radial deformations as they were measured during the experiments, the results of the numerical models were set to the reference experiments.

2. *The approximation of the contact area of the diffusion bonding with the electrical resistance*

I introduced for the diffusion bonding model a contact electrical resistance function, with decreasing tendency as $R_{contact} = k_1 \cdot e^{-k_2 \cdot t}$ [Ω]. The function was adjusted to the diffusion bonding in the numerical model, where this function was the principal difference compared to the reference model.

I found that the contact electrical resistance at the mating surfaces of the bonding influences significantly the heat distribution. I proved that the contact electrical resistance during the diffusion bonding decreases the axial deformation compared to the reference experiments in a measurable way.

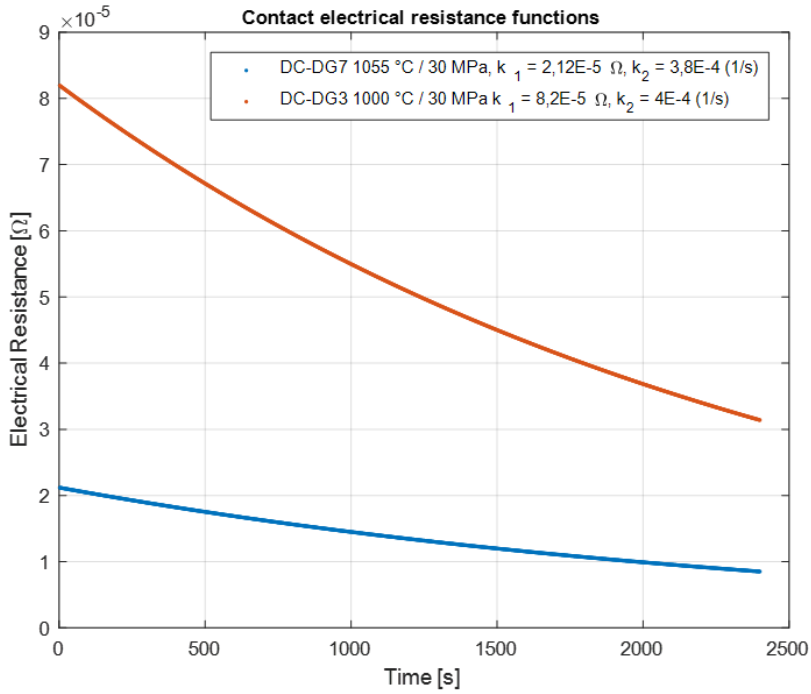

The contact electrical resistance functions used for the numerical modelling were defined for the two diffusion bonding experiments

3. *Application of the Hill and Wallach model and the Zhang contact electrical resistance equation*

I carried out a theoretical diffusion bonding modelling for the contact surface based on the theories by Hill and Wallach (1989). According to the model, after 10-20 min the bonded area reaches the 90% similarly to the earlier results by Hill (1983) for 316L. I found based on the modelling and the experiences from the literature that we can expect in the reality slower and ambiguous results for the bonded area compared to the theory.

Based on the Zhang (2012) model, I determined the contact electrical resistance in function of the bonded area to the bonded specimen surfaces. I introduced that the contact electrical resistance function was derived by my own numerical model and the results from the Zhang model were in the same order of magnitude, in this way they were comparable to each other.

I proved with the Hill and Wallach and Zhang models that the contact electrical resistance is a good marker for diffusion bonded area during the bonding process.

4. *Determination of the contact (bonded) area by measurements and by theoretical modelling*

I determined the increasing bonded area in time using the Zhang model on the contact electrical resistance which was defined by the own numerical simulation. In this way, I made examinable the progress of a long diffusion bonding instead of stopping the bonding process.

Comparing the numerical model of the experiments and the Hill and Wallach theory, I found that the experiments gave smaller bonded area than expected. I found that in both cases (experiment, theory) the bonding with higher temperature (1055 °C) gave higher bonded area compared to the bonding at lower temperature (1000 °C).

With these, I worked out a new method with the experiments on the applied physical simulator to determine the bonded area during the diffusion bonding. I made comparable the bonded area between the results were determined by the experiments through the own numerical model and the results coming from the existing theoretical models.

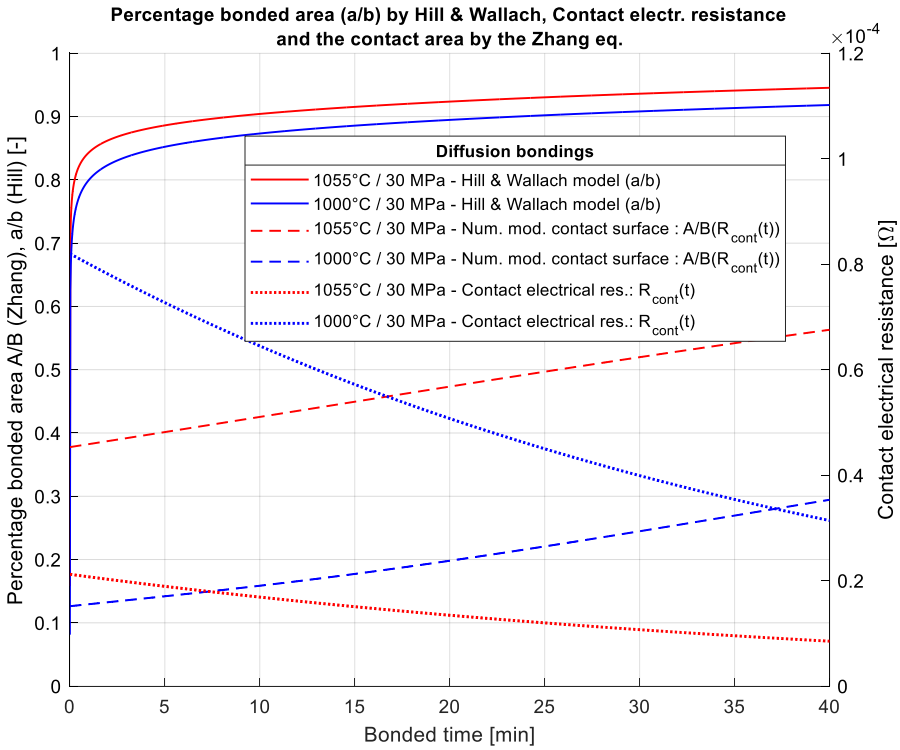

The diffusion bonded area (a/b) by the Hill and Wallach model comparing with the results were derived by the Gleeble numerical modelling and calculated by the Zhang equations: $A/B(R_{cont}(t))$

5. CONCLUSION AND SUGGESTIONS

During my research I dealt with diffusion bonding of 316L stainless steel specimens which are used in the ITER tokamak and in other nowadays operating tokamaks.

I proved that by the electrical resistance heating made diffusion bonding experiments with the reference experiments were able to investigate the diffusion bonding process. I found connection between the axial alteration of diffusion bonding and reference samples and between the progress of the diffusion bonding. The experiments were carried out with same parameters: 1000 °C / 30 MPa / 60 min, and 1055 °C / 30 MPa / 40 min.

I developed a new numerical model, which were able to calculate the heat distribution on a half specimen and the axial deformations of the specimens. The model was set to the reference tests. In future I suggest and plan to modify the numerical model in many points. Following the high temperature regime (900 °C – 1100 °C) I suggest using the plastic deformation to calculate the axial deformation according to Lindgren et al. (2017) results. Based on the literature yield stress limit will reduce and the creep may increase if high DC current is led through a specimen. I suggest investigating the alteration of the yield stress with the Gleeble simulator together with the results were worked out by Varga (2020).

I prepared the diffusion bonding model based on Hill and Wallach (1989) results. With the results I suggest defining a more precise upper and lower limit for 316L (temperature, pressure, time), and the possibility to substitute the parameters to each other. I suggest carrying out the more precise model for 316L was presented by Ruifang (2012), which was developed for the alloy TC4 (Ti-6Al-4V). Related to the modelling the 3D ellipsoid surface (by Zhang, 2018) may give more realistic results as the 2D ellipse infinite grooves.

The theoretical modelling can give very useful results if they can extend to the diffusion bonding of different material pairs. However, it requires more severe research of the theory.

Beyond the 316L stainless steel I suggest applying the Hill and Wallach model to the EUROFER 97 and similar ODS steels as well.

In numerical simulation further studies are planned to find a clear connection between the contact electrical resistance by Zhang (2012) model at bonding surface and the voids appeared on mating surface modelled by Hill, Wallach (1989). These studies can be a base on a new non-destructive test method.

6. SUMMARY

Diffusion bonding and reference heat affected zone tests on 316L specimens were performed in a Gleeble 3800 GTC physical simulator at the University of Dunaújváros. The cylindrical specimens had 30+30 mm and 60 mm useful length. Selecting two pairs I prepared detailed numerical simulations for comparison on the diffusion bonding and the reference experiments.

1 D heat conduction model using the material's creep properties were developed to estimate the sample axial deformation, where the bonding parameters were the followings: 1000 °C / 30 MPa / 60 min, and 1055 °C / 30 MPa / 40 min. The numerical simulation was able to estimate the axial and radial deformation, the used DC current, and the contact electrical resistance raised on the mating surfaces. The numerical simulation took into account the material properties, the axial force for the constant applied pressure, and the DC current, as it was controlled by Gleeble system for the constant temperature. These results were published in Baross et al. (2020, 2022), the preparatory calculations, partial results and laboratory tests were published in Baross et al. (2015, 2017, 2018, 2019) articles.

In the physical tests we could observe the stroke differences as they occurred between physical tests and the reference tests at same parameters. These phenomena were shown in the numerical modelling with the additional contact electrical resistance at the mating surface. In this way the surface contact resistance could be estimated by the physical simulations and because of the strong dependencies of the creep parameters on the temperature. With these I have found connection between the contact electrical resistance and the progress during the diffusion bonding process.

The theoretical diffusion bonded area was modelled by Hill and Wallach (1989). However, the first estimations published in Baross et al. (2018) underestimated the contact resistance, but the contact electrical resistance by the Zhang (2012) equation gave much larger resistance following the significant constriction resistance. These results gave similar order of magnitude to the earlier determined functions by the help of the physical experiments (Baross et al., 2020, 2022).

I think the further study of the contact electrical resistance and the diffusion bonded area grow may result a new method to investigate the diffusion bonding process.

7. MOST IMPORTANT PUBLICATIONS RELATED TO THE THESIS

Referred articles in foreign languages

1. **Baross, T.**, Bereczki, P., Jánosi, L., Palánkai, M., Sánta, B., Veres, G. (2020): Diffusion bonding experiments of 316L steels in a Gleeble 3800 thermomechanical simulator for investigation of non-destructive inspection methods, Fusion Engineering and Design, Vol. 160, 111768, ISSN 0920-3796, https://doi.org/10.1016/j.fusengdes.2020.111768 http://www.sciencedirect.com/science/article/pii/S0920379620303161 (IF : 1,692 2020)

2. **Baross, T.**, Biel, W., Krejczinger, A., Krasikov, Yu., Panin, A. (2013): Retractable tube design issues in ITER CXRS UPP #3, Fusion Engineering and Design, Vol. 88, Issues 6–8, Pages 1352-1356, ISSN 0920-3796, https://doi.org/10.1016/j.fusengdes.2013.02.105., https://www.sciencedirect.com/science/article/pii/S0920379613002202) (IF: 1,453 2013)

3. Krasikov, Yu., **Baross, T.,** Biel, W., Litnovsky, A., Hawkes, N., Kiss, G., Klinkhamer, J.F.F., Koning, J.F., Krimmer, A., Neubauer, O., Panin, A. (2011): Development of design options for the port plug components of the ITER core CXRS diagnostic, Fusion Engineering and Design, Volume 86, Issues 9–11, Pages 2055-2059, ISSN 0920-3796, https://doi.org/10.1016/j.fusengdes.2011.01.086. (https://www.sciencedirect.com/science/article/pii/S0920379611000986) (IF: 1,49 2011)

4. Mertens, Ph., Castaño Bardawil D. A., **Baross, T.**, Biel W., Friese, S., Hawkes, N., Jaspers, R.J.E., Kotov, V., Krasikov, Yu., Krimmer, A., Litnovsky, A., Marchuk, Olaf Neubauer, O., Offermanns, G., Panin., A., Pokol, G., Schrader, M., Samm, U. (2015): Status of the R&D activities to the design of an ITER core CXRS diagnostic system, Fusion Engineering and Design, Vol. 96–97, Pages 129-135, ISSN 0920-3796, https://doi.org/10.1016/j.fusengdes.2015.05.039. (https://www.sciencedirect.com/science/article/pii/S0920379615300028) (IF: 1,301 2015)

5. **Baross, T**., De Baets, P., Veres, G. (2017): Development of structural materials for fusion reactors, Scientific Bulletin, Serie C, Fascicle: Mechanics, Tribology, Machine Manufacturing Technology, pp. 13-16., ISSN 1224-3264

6. **Baross, T.**, Jánosi, L., Kalácska, G., Veres, G. (2015): Diffusion bonding of plasma facing components of fusion reactor (ITER), Mechanical Engineering Letters, Szent István University, Vol. 12, pp. 101-109., HU ISSN 2060-3789

7. **Baross, T.**, Jánosi, L. and Veres, G. (2017): Analytical and numerical model of the temperature distribution of diffusion welding specimens on a Gleeble 3800 thermomechanical simulator, Mechanical Engineering Letters, Szent István University, Vol. 15, pp. 16-26., HU ISSN 2060-3789

8. **Baross, T.**, Bereczki, P., Jánosi, L., Palánkai, M., Sánta, B., Veres, G. (2019): Non-destructive inspection methods of diffusion bonding on 1.4404 specimens welded in a Gleeble 3800 thermomechanical simulator, Synergy International Conferences - Engineering, Agriculture and Green Industry Innovation Gödöllő, Hungary, November 4-6., Mechanical Engineering Letters, Szent István University, Vol. 18, pp. 17-26., HU ISSN 2060-3789

9. **Baross, T.**, Jánosi, L., Veres, G. (2018): Plastic deformation and heat generation rate at the contact surface during diffusion bonding at Gleeble 3800 thermomechanical simulator, Mechanical Engineering Letters, Szent István University, Vol. 17, pp. 37-46., HU ISSN 2060-3789

Referred articles in Hungarian

10. **Baross, T.**, Bereczki, P., Jánosi, L., Palánkai, M., Veres, G. (2022): 316L mintákon végzett diffúziós hegesztési kísérletek Gleeble 3800 fizikai szimulátoron, Nukleon, XV. évf. (2022) 241, ISSN: 1789-9613